Distinctive g-factor of moiré-confined excitons in van der Waals heterostructures

Y. Galvão Gobato,[*,†] C. Serati de Brito,[†] A. Chaves,[*,‡,¶] M. A. Prosnikov,[§] T. Woźniak,[‖] Shi Guo,[⊥] Ingrid D. Barcelos,[#] M. V. Milošević,[¶] F. Withers,[⊥] and P. C. M. Christianen[§]

†*Physics Department, Federal University of São Carlos (UFSCAR)-Brazil*
‡*Universidade Federal do Ceará, Departamento de Física, 60455-760 Fortaleza, Ceará, Brazil*
¶*Department of Physics, NANOlab Center of Excellence, University of Antwerp, Belgium*
§*High Field Magnet Laboratory (HFML–EMFL), Radboud University, 6525 ED, Nijmegen, The Netherlands*
‖*Department of Semiconductor Materials Engineering, Wrocław University of Science and Technology, 50-370 Wrocław, Poland*
⊥*Centre for Graphene Science, College of Engineering, Mathematics and Physical Sciences, University of Exeter, Exeter, EX4 4QF*
#*Brazilian Synchrotron Light Laboratory (LNLS), Brazilian Center for Research in Energy and Materials (CNPEM), 13083-970 Campinas, São Paulo, Brazil*

E-mail: yara@df.ufscar.br; andrey@fisica.ufc.br

Abstract

We investigated the valley Zeeman splitting of excitonic peaks in the micro-photoluminescence (μPL) spectra of high-quality hBN/WS_2/$MoSe_2$/hBN heterostructures under perpendicular magnetic fields up to 20 T. We identify two neutral exciton peaks in the μPL spectra: the lower energy one exhibits a reduced g-factor relative to that of the higher energy peak, and much lower than the recently reported values for interlayer excitons in other van der Waals (vdW) heterostructures. We provide evidence that such a discernible g-factor stems from the spatial confinement of the exciton in the potential landscape created by the moiré pattern, due to lattice mismatch and/or inter-layer twist in heterobilayers. This renders magneto-μPL an important tool to reach deeper understanding of the effect of moiré patterns on excitonic confinement in vdW heterostructures.

Keywords

Twisted van der Waals Heterostructures, TMDs, Moiré Excitons, Magneto-Optics.

Recent years have witnessed enormous interest in the optical properties of heterostructures based on monolayer transition-metal dichalcogenides (TMDs).[1,2] They exhibit a direct band gap at two inequivalent ±K valleys and enhanced excitonic effects.[3–9] The $\pm K$ valleys can be individually addressed using right- (σ_+) and left-handed (σ_-) circularly polarized light.[10] Under perpendicular external magnetic fields, valley Zeeman effects and magnetic-field-induced valley polarization can be observed.[11–18]

TMD heterostructures with stacking angles near either 0° (AA stacking) or 60° (AB stack-

ing) exhibit pronounced emission from both inter-layer and intra-layer excitons.[19–26] The lattice mismatch between the materials that form the heterostructure, combined with small inter-layer twist angles, lead to a moiré pattern consisting of regions where the crystal exhibits stacking registries that are locally different along the materials plane.[27]

The effective g-factor of inter-layer excitons (iXs) depends on the twist angle between the layers of van der Waals heterostructures (vdWHSs).[28] Several experimental studies of $MoSe_2/WSe_2$ heterostructures have shown an effective g-factor of iXs of $g \approx +6$ for twist angles near 0°, while $g \approx -15$ was found for twist angles around 60°.[21,28,29] These values are very different from reported g-factors of intra-layer excitons in individual monolayer TMDs ($g \approx -4$).[12,14,15,28] In fact, the value of the effective exciton g-factor results from the spin and orbital angular momenta of the electron and the hole bands, while its sign is governed by optical selection rules.[30,31] Therefore, it is significantly affected by the materials composition, inter-layer exciton hybridization, and even by the spread of the exciton wave function.[32] In the presence of the effective confining potential produced by the moiré pattern, the confined exciton wave function in reciprocal space is expected to populate regions away from the K-point edge of the Brillouin zone, thus effectively modifying the exciton g-factor, which in turn can be used to probe the moiré exciton confinement.

There is currently a controversy in the literature, regarding the nature of the lower energy moiré exciton peak in the optical emission of a $MoSe_2/WS_2$ heterostructure.[33–36] It was shown that the conduction band is nearly degenerate for the two constituent layers and the excitonic bands of intra- and interlayer excitons could hybridize, resulting in a resonant enhancement of the moiré superlattice effects. Therefore, the observed lower energy exciton peak in the PL spectrum was previously attributed to a hybridized intra- and interlayer exciton.[34,35] Recent reflectance contrast experiments of gated heterostructures[33] evidenced that the hybridization of intra- and interlayer-excitons is weak for the lower energy exciton peak, which has considerable impact on theoretical predictions of the exciton g-factors for samples with twist angles around 0° and 60°.

In this work, we investigate the exciton g-factors in a $MoSe_2/WS_2$ heterobilayer with twist angles around 0° and 60°. Our magneto-micro-photoluminescence (magneto-μPL) data reveal the existence of two neutral exciton peaks, at different energies. The effective g-factor of the lower-energy exciton is consistently lower as compared to either the perfectly charge-separated inter-layer excitons observed in $MoSe_2/WSe_2$ (and other) heterobilayers, or the intra-layer excitons either in an individual $MoSe_2$ monolayer or in $MoSe_2/WS_2$ heterobilayers. We argue that the low energy PL peak is due to an exciton whose center-of-mass motion is confined by the moiré potential landscape, as evidenced by its energy separation from the peak identified as the $MoSe_2$ intra-layer exciton (with an experimentally validated g-factor).

As shown in Fig. 1(a), the PL spectrum of the $MoSe_2/WS_2$ vdWHS exhibits two peaks associated to the neutral excitons, labeled mX (1.603 eV) and X_A (1.646 eV), interspersed by trion peaks mX* (1.570 eV) and X* (1.619 eV). These results are very similar to previous experimental results reported for $MoSe_2/WS_2$ heterobilayers.[34,35] We found the energy separation between the mX and X_A PL peak positions of $\approx$ 43 meV. The energy separation between X_A and X* is 27 meV, whereas between mX* and mX peaks a splitting of 33 meV was observed. The energy separations are consistent with the identification of mX* and X* as trion emissions. Our laser power dependence study of all observed PL bands at 4 K (Fig. S3 in the Supplementary Material (SM)[37]) provides further support to this interpretation of the excitonic nature of the different PL peaks. We thus correlate the experimentally observed mX peak to a moiré-confined exciton state, whereas the X_A peak is interpreted as the emission from an unconfined intra-layer $MoSe_2$ exciton,[33–35] as will be detailed further below.

In order to understand the origin of the two neutral exciton peaks consistently observed in our experiments, let us consider a van der Waals

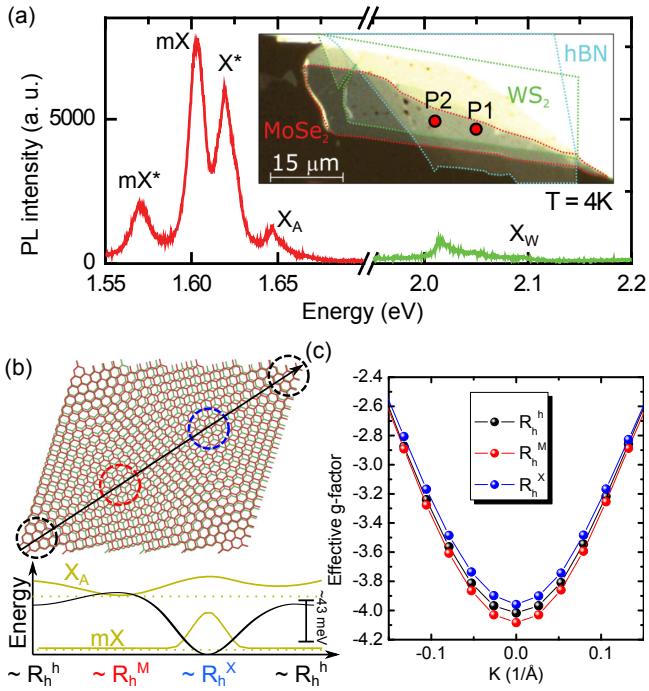

Figure 1: (a) Typical PL spectrum of the $MoSe_2/WS_2$ vdWHS at 4 K with twist angle around 0° at the position P2 indicated in the inset. The inset shows the optical image of the sample. The intersection of red ($MoSe_2$) and green (WS_2) delimited areas highlights the vdWHS region. PL of the monolayer WS_2 region of the sample (green data points) shows features at higher energies, identified as the monolayer exciton X_W peak for this material, whereas the lower energy features are identified as the free (moiré-confined) $MoSe_2$ intra-layer exciton X_A (mX) and trion X^* (mX^*). (b) Sketch of the crystal structure of a $MoSe_2/WS_2$ vdWHS with a twist angle $\approx 0°$. Local stacking registries R_h^h, R_h^M and R_h^X, highlighted respectively by black, red, and blue circles, form a periodic moiré pattern. The quasi-particle energy gap is locally different in each of these regions, thus producing a moiré potential landscape for excitons. This is illustrated by the black line in the bottom panel, which depicts the quasi-particle gap along the arrow drawn in the top panel. The mX and X_A peaks in the PL spectrum originate respectively from confined and (nearly) free excitons in the moiré pattern, whose wave functions are represented by yellow curves in the bottom panel. (c) Effective g-factor dispersion for the intra-layer $MoSe_2$ exciton as a function of its momentum K, as obtained by DFT calculations assuming the three stacking registries identified in (b).

stacked $MoSe_2/WS_2$ hetero-bilayer with interlayer twist angle $\approx 0°$, as sketched in Fig. 1(b). The periodic moiré pattern created by the lattice mismatch between the layers exhibits regions with local stacking registries identified as R_h^h, R_h^M and R_h^X, marked as black, red, and blue circles, respectively. Since the quasi-particle gap of each of these registries is different, one expects these regions to form a periodic landscape of potential wells and barriers for the exciton,[38] as illustrated by the black line in the bottom panel of Fig. 1(b). The quasi-particle gaps obtained from ab initio calculations with hybrid functional (HSE06) in a $MoSe_2/WS_2$ vdWHS with R_h^h, R_h^M and R_h^X are 1.830 eV, 1.831, and 1.816 eV, respectively. All three cases exhibit practically the same effective mass and, consequently, the same binding energy of 0.230 eV, thus explaining the experimentally observed peaks around 1.6 eV. In the R_h^X case, however, the theoretically predicted exciton energy is at least 15 meV lower than those of R_h^h and R_h^M, thus working as a confining well for the exciton center-of-mass. Since the inter-atomic distances in the actual vdWHS crystal are likely different from those in our simulations for pure R_h^h, R_h^M and R_h^X crystals, which were artificially strained to produce commensurate lattices, and our calculations for local quasi-particle gaps were made without GW corrections, the actual moiré confinement potential in the $MoSe_2/WS_2$ vdWHS is likely to be significantly stronger than the $\approx$15 meV predicted here.

The valence band edges of the isolated monolayers are separated by $\approx$ 750 meV,[39] which restricts the holes in the lowest energy exciton states to the $MoSe_2$ layer. Conversely, the conduction band offset between the individual monolayers is small: for instance, Refs. [34] and [35] suggest conduction band offsets of 13 meV and 5.8 meV, respectively, with lowest energy electrons also in the $MoSe_2$ layer. Ab initio calculations in Ref. [39] give somewhat higher values for this band offset, but all results in the literature point towards a type-I band alignment for this combination of materials.[33,40] Therefore, the lowest energy exciton state in this vdW HS must have a dominant intra-layer $MoSe_2$ component, although, due to

such low conduction band offset, hybrid states with an inter-layer component, where electrons partially populate the WS_2 layer as well, may also be possible.Consequently, we will focus on the effect of in-plane moiré confinement on the g-factor of intra-layer exciton .

In the presence of a perpendicularly applied magnetic field $\vec{B} = B\hat{z}$, the energy of each exciton state shifts as

$$E_i(B) = E_i(0) \pm g_i \mu_B B/2, \qquad (1)$$

where μ_B is the Bohr magneton, B the magnetic field strength, i = mX, mX*, X* or X$_A$, the $\pm$ sign depends on the valley degree of freedom, associated with the circular polarization $\sigma_\pm$, and the linear term corresponds to the Zeeman shift, with an effective Landé g-factor g_i. The quadratic (diamagnetic) shifts for each exciton state are an order of magnitude lower than the Zeeman shifts and are therefore neglected. These g-factors are directly related to the angular momenta of the valence and conduction band states involved in the exciton transition. Although a survey of such angular momenta values for several monolayer TMDs, along with a thorough description of the calculation method, can be found in Ref. [30], we briefly describe the theoretical procedure to obtain effective exciton g-factors from density functional theory calculations in the SM,[37] for the sake of completeness.

Results in Fig. 1(c) demonstrate that the angular momenta of the conduction and valence band states in a $MoSe_2/WS_2$ vdWHS with three different stacking registries observed for $\approx 0°$ twist angle in Fig. 1(b) are not significantly different from that of the isolated $MoSe_2$ monolayer, which is $g \approx -4$.[30] On the other hand, they are strongly reduced in modulus for exciton momenta away from the exciton band edge. In fact, the momentum of a ground-state exciton that is quantum confined by an external potential is naturally non-zero. The moiré potential illustrated in the bottom panel of Fig. 1(b), with minima at the R_h^X regions, suggests that the exciton center-of-mass is effectively quantum confined to these regions, which allows one to predict a significant reduction in the g-factors for moiré confined exciton states. Wave functions of shallow (X$_A$) and (mX) confined exciton states are depicted by yellow lines in the bottom panel of Fig. 1(b).

Figure 2 (a) shows a typical PL spectra for left (σ_-) and right (σ_+) circularly polarized emissions and (b) the magnetic field dependence of the PL spectrum for both polarized emissions under magnetic field up to 20 T for the position P1, marked in Fig. 1(a). A red/blue shift of the circularly polarized σ_+/σ_- PL peak positions was observed with increasing magnetic field, which clearly evidences the regular valley Zeeman splitting effect.[11–18] Similar behavior was observed for μPL data obtained at different laser positions of the heterostructure (see Figs. S4 and S5 in the SM[37]).

We have determined the peak energies of the emission lines as a function of magnetic field by fitting each PL peak with a Voigt line shape. The effective g-factors for all emission peaks are obtained by fitting the experimental Zeeman splitting to $\Delta E_i = E_i^{\sigma_+} - E_i^{\sigma_-} = g_i \mu_B B$ (Fig. 2). This yields g-factors ≈-4.4 for both the X$_A$ and X* PL peaks. Lower g-factors are observed for the mX* trion and mX exciton, with values $g_{mX^*} = -3.3$ and $g_{mX} = -3.5$, respectively. These values are also lower than the effective g-factors of excitons in monolayer $MoSe_2$, with $g_A \approx -4$ in previous works.[41]

As previously discussed, moiré confined excitons are expected to exhibit reduced g-factors. We therefore address the X$_A$ peak as either free or shallow-confined exciton states in the higher energy R_h^h and R_h^M regions, whereas mX is interpreted as a moiré-confined exciton state at the R_h^X region, with lower energy and, consequently, non-zero center-of-mass momentum. This interpretation of X$_A$ and mX matches the findings of earlier works,[34] except for our assumption of weak inter-layer hybridization in mX, in accordance with Ref. [33].

Let us compare the experimentally observed $\approx 22\%$ difference between g_A and g_{mX} with the theoretical predictions in Fig. 1(c). The predicted g-factor for nearly free intra-layer $MoSe_2$ excitons is $g_A \approx -4$. A 22% lower value for the moiré exciton yields $g_{mX} \approx -3.12$ which, according to Fig. 1(c), requires an ex-

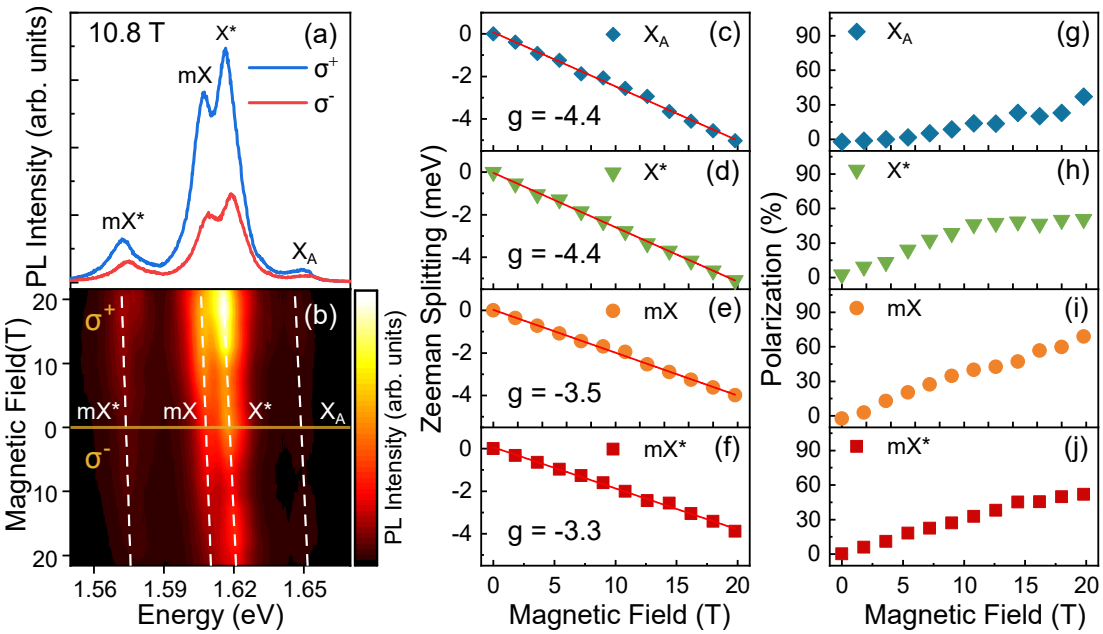

Figure 2: (a) Typical PL spectra of σ_+ and σ_- light polarizations at 10.8 T and 4 K for the $MoSe_2/WS_2$ vdWHS with a twist angle around 0°, at position P1. (b) color-code map of the PL intensity versus energy and magnetic field for σ_- and σ_+ light polarizations. (c) - (f) Magnetic field dependence of the valley Zeeman splitting of each PL peak as a function of magnetic field. Solid lines are linear fits to the data. (g)-(j) Magnetic field dependence of the valley polarization for each PL peak.

citon momentum $K \approx 0.11$ Å^{-1}. This corresponds to a confined state with energy roughly $\hbar^2K^2/2M \approx 40$ meV below that of the free exciton, where we used the total exciton effective mass $M = m_e + m_h = 1.094m_0$, as obtained from DFT. Indeed, this is in excellent agreement with the experimentally observed 43 meV separation between X_A and mX exciton peaks in the PL spectra. Moreover, this energy is also in the same order of magnitude as the one observed for similar moiré-confined excitons in Ref. [38].

The degree of valley polarization, defined as $P = (I^{\sigma+} - I^{\sigma-})/(I^{\sigma+} + I^{\sigma-})$, is shown in Figure 2 as a function of the field for each excitonic peak under circular polarization excitation. The mX excitons exhibit a circular polarization as large as $\approx 70\%$ at a field of 20 T, a nearly twice stronger polarization compared to the free X_A exciton at this field. The high polarization degree for mX suggests an increase of intervalley scattering times for the moiré confined exciton. However, further studies would be necessary to understand in more detail the polarization degree of the moiré confined exciton.

Despite the qualitative agreement between the g-factors of the different mX and X_A peaks observed in our μPL experiment and their theoretically predicted values, the latter are quantitatively lower in magnitude. In fact, g-factors of X_A in $MoSe_2$ and WS_2 monolayers obtained by ab initio calculations are slightly underestimated as compared to existing experimental data in the literature.[30] Nevertheless, our model shows that the distinctly lower g-factors for the mX states is due to the exciton wave function quantum confinement by the moiré pattern.

If there was an important effect of inter-layer hybridization for mX[34] for this vdWHS, our DFT calculations predict an even lower exciton g-factor, as a consequence of the lower angular momentum for conduction band electrons in the WS_2 layer.[37] However, as the hybridization is weak, the exciton g-factors observed here in $MoSe_2/WS_2$ vdWHS are similar or even reduced as compared to those of excitons in

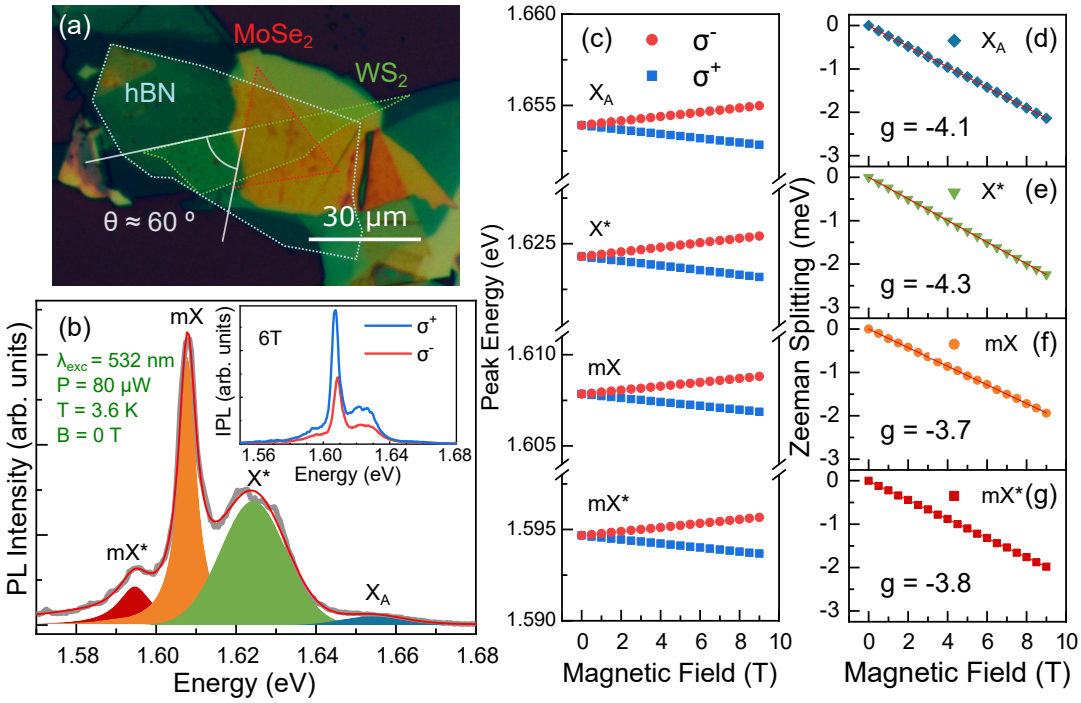

Figure 3: (a) Optical image of hBN-encapsulated $MoSe_2/WS_2$ vdWHS with a twist angle around 60°. (b) PL spectrum and typical PL fitting at 0T. The inset shows σ_+ and σ_- PL spectra at 6 T. (c) Magnetic field dependence of the PL peak energies for σ_+ and σ_- polarizations (d)-(g) Zeeman splitting for each PL peak as a function of magnetic field. Solid lines are linear fits to the data. The corresponding extracted effective g-factors are indicated in the panels (d)-(g).

monolayer $MoSe_2$, in contrast to the g-factors of excitons in other similar heterostructures, such as $MoSe_2/WSe_2$ vdWHS,[28] where exciton g-factors in the vdWHS are rather *enhanced* as compared to those of either monolayer $MoSe_2$ or WSe_2. Furthermore, for twist angles around 60°, the inter-layer exciton g-factors would be expected to be higher due to the sign change of the angular momentum for the conduction band states for these excitons.[28,30] However, since the mX and X_A states in $MoSe_2/WS_2$ vdWHS have a strong intra-layer component and low inter-layer contribution,[33] our model estimates the g-factors in $\theta \approx 60°$ twisted $MoSe_2/WS_2$ heterostructures to be similar to those for $\theta \approx 0°$, in contrast to $MoSe_2/WSe_2$ vdWHS. Indeed, we experimentally verified this prediction with a $MoSe_2/WSe_2$ vdWHS sample with twist angle 60°. Figure 3 (a) shows the optical image of this sample. The PL spectrum at zero field and a typical spectrum under magnetic field is shown in Figure 3 (b). We observed a sharp mX peak at around 1.608 eV, and an exciton peak at around 1.654 eV. Therefore, the energy separation between the X_A and mX exciton peak is 46 meV. Figure 3 (c-g) shows the magnetic field dependence of the PL peak energies for the σ_+ and σ_- polarizations and the Zeeman splitting for all emission peaks. The corresponding effective g-factor for mX is around -3.7 which is close to the value obtained for the sample with twist angle 0°. In general, for all samples we have observed a small reduction of g-factors for mX and mX*, as compared to X_A and X* peaks. This result is in agreement with our theoretical predictions for moiré confined excitons with a dominant intralayer component.

In conclusion, we have measured the polarization-resolved photoluminescence of exciton states in high quality hBN-encapsulated $MoSe_2/WS_2$ heterostructures with twist angles around 0° and 60°, and under perpendicular magnetic fields up to 20 T. Two neutral excitons are identified: the free exciton state, with higher energy, whereas the moiré-confined exciton with lower energy. The energy separation

between these PL peaks suggests a moiré confinement energy of 43-46 meV, with respect to the free exciton state, which matches with our theoretical estimates. Furthermore, the moiré-confined exciton exhibits reduced g-factor. In addition, similar values for the g-factors were obtained for samples with twist angles around 0° and 60°, which indicates a weak hybridization effect between intralayer and interlayer excitons. The observed reduction of the g-factor value for the moiré exciton is a consequence of the quantized center-of-mass momentum of the moiré-confined exciton, which makes it probe regions of the Brillouin zone where the angular momentum state of the electron-hole pair is significantly reduced, as demonstrated by our calculations. Overall, we expect that our result of distinctive g-factors for moiré-trapped excitons will yield an important contribution to the ongoing debate, stimulating the development of improved theoretical models for the vdW heterostructures with moiré potentials therein.

Acknowledgement This work was supported by HFML-RU/NWO-I, member of the European Magnetic Field Laboratory (EMFL). This work was also financially supported by the Brazilian Council for Research (CNPq), through the PRONEX/FUNCAP, Universal, and PQ programs (311678/2020-3), and the Research Foundation - Flanders. CSB acknowledges the financial support from CAPES fellowship. YGG acknowledges the financial support from FAPESP (grants 2018/01808-5 and 2019/23488-5), CNPQ (grants 311678/2020-3 and 426634/2018-7) and the Brazilian Synchrotron Light Laboratory (LNLS) for the LAM support facility. IDB acknowledges the financial support from FAPESP (grants 2019/14017-9) and CNPq (grants 311327/2020-6). TW acknowledges financial support from National Science Centre, Poland under grant 2021/41/N/ST3/04516. DFT calculations were performed with the support of the Interdisciplinary Centre for Mathematical and Computational Modelling (ICM) University of Warsaw and Center for Information Services and High Performance Computing (ZIH) at TU Dresden.

Supporting Information Available

The following files are available free of charge.

- SM: Sample preparation and experimental methods; PL spectra for different positions on the sample with 0° stacking angles; Fitting of PL spectra measured at position P2 ; Laser power dependence of the PL spectra; Color-code mapping of the magnetic field dependence of σ^+ and σ^- PL with stacking angle close to 0°; Zeeman splitting and magnetic induced valley polarization, at position P2; TRPL measurements for the $\approx 0°$ stacking angle sample; Theoretical model for exciton g-factors. (PDF)

References

(1) Geim, A. K.; Grigorieva, I. V. Van der Waals heterostructures. *Nature* **2013**, *499*, 419–425.

(2) Novoselov, K.; Mishchenko, A.; Carvalho, A.; Neto, A. C. 2D materials and van der Waals heterostructures. *Science* **2016**, *353*.

(3) Mak, K. F.; Lee, C.; Hone, J.; Shan, J.; Heinz, T. F. Atomically thin MoS2: A new direct-gap semiconductor. *Physical Review Letters* **2010**, *105*, 2–5.

(4) Splendiani, A.; Sun, L.; Zhang, Y.; Li, T.; Kim, J.; Chim, C. Y.; Galli, G.; Wang, F. Emerging photoluminescence in monolayer MoS2. *Nano Letters* **2010**, *10*, 1271–1275.

(5) Xu, X.; Yao, W.; Xiao, D.; Heinz, T. F. Spin and pseudospins in layered transition metal dichalcogenides. *Nature Physics* **2014**, *10*, 343–350.

(6) Xiao, D.; Liu, G. B.; Feng, W.; Xu, X.; Yao, W. Coupled spin and valley physics in monolayers of MoS 2 and other group-VI dichalcogenides. *Physical Review Letters* **2012**, *108*, 1–5.

(7) Mak, K. F.; He, K.; Shan, J.; Heinz, T. F. Control of valley polarization in monolayer MoS2 by optical helicity. *Nature Nanotechnology* **2012**, *7*, 494–498.

(8) Zeng, H.; Dai, J.; Yao, W.; Xiao, D.; Cui, X. Valley polarization in MoS 2 monolayers by optical pumping. *Nature Nanotechnology* **2012**, *7*, 490–493.

(9) Schaibley, J. R.; Yu, H.; Clark, G.; Rivera, P.; Ross, J. S.; Seyler, K. L.; Yao, W.; Xu, X. Valleytronics in 2D materials. *Nature Reviews Materials* **2016**, *1*, 1–15.

(10) Ishii, S.; Yokoshi, N.; Ishihara, H. Optical selection rule of monolayer transition metal dichalcogenide by an optical vortex. Journal of Physics: Conference Series. 2019; p 012056.

(11) Aivazian, G.; Gong, Z.; Jones, A. M.; Chu, R. L.; Yan, J.; Mandrus, D. G.; Zhang, C.; Cobden, D.; Yao, W.; Xu, X. Magnetic control of valley pseudospin in monolayer WSe 2. *Nature Physics* **2015**, *11*, 148–152.

(12) Li, Y.; Ludwig, J.; Low, T.; Chernikov, A.; Cui, X.; Arefe, G.; Kim, Y. D.; Zande, A. M. V. D.; Rigosi, A.; Hill, H. M.; Kim, S. H.; Hone, J.; Li, Z.; Smirnov, D.; Heinz, T. F. Valley splitting and polarization by the zeeman effect in monolayer MoSe2. *Physical Review Letters* **2014**, *113*, 1–5.

(13) Srivastava, A.; Sidler, M.; Allain, A. V.; Lembke, D. S.; Kis, A.; Imamoglu, A. Valley Zeeman effect in elementary optical excitations of monolayer WSe 2. *Nature Physics* **2015**, *11*, 141–147.

(14) Macneill, D.; Heikes, C.; Mak, K. F.; Anderson, Z.; Kormányos, A.; Zólyomi, V.; Park, J.; Ralph, D. C. Breaking of valley degeneracy by magnetic field in monolayer MoSe2. *Physical Review Letters* **2015**, *114*, 1–5.

(15) Wang, G.; Bouet, L.; Glazov, M. M.; Amand, T.; Ivchenko, E. L.; Palleau, E.; Marie, X.; Urbaszek, B. Magneto-optics in transition metal diselenide monolayers. *2D Materials* **2015**, *2*, 34002.

(16) Mitioglu, A. A.; Plochocka, P.; Aguila, G. D.; Christianen, P. C.; Deligeorgis, G.; Anghel, S.; Kulyuk, L.; Maude, D. K. Optical Investigation of Monolayer and Bulk Tungsten Diselenide (WSe2) in High Magnetic Fields. *Nano Letters* **2015**, *15*, 4387–4392.

(17) Stier, A. V.; McCreary, K. M.; Jonker, B. T.; Kono, J.; Crooker, S. A. Exciton diamagnetic shifts and valley Zeeman effects in monolayer WS2 and MoS2 to 65 Tesla. *Nature Communications* **2016**, *7*, 1–8.

(18) Plechinger, G.; Nagler, P.; Arora, A.; Águila, A. G. D.; Ballottin, M. V.; Frank, T.; Steinleitner, P.; Gmitra, M.; Fabian, J.; Christianen, P. C.; Bratschitsch, R.; Schüller, C.; Korn, T. Excitonic Valley Effects in Monolayer WS2 under High Magnetic Fields. *Nano Letters* **2016**, *16*, 7899–7904.

(19) Rivera, P.; Seyler, K. L.; Yu, H.; Schaibley, J. R.; Yan, J.; Mandrus, D. G.; Yao, W.; Xu, X. Valley-polarized exciton dynamics in a 2D semiconductor heterostructure. *Science* **2016**, *351*, 688–691.

(20) Nayak, P. K.; Horbatenko, Y.; Ahn, S.; Kim, G.; Lee, J. U.; Ma, K. Y.; Jang, A. R.; Lim, H.; Kim, D.; Ryu, S.; Cheong, H.; Park, N.; Shin, H. S. Probing Evolution of Twist-Angle-Dependent Interlayer Excitons in MoSe2/WSe2 van der Waals Heterostructures. *ACS Nano* **2017**, *11*, 4041–4050.

(21) Nagler, P.; Ballottin, M. V.; Mitioglu, A. A.; Mooshammer, F.; Paradiso, N.; Strunk, C.; Huber, R.; Chernikov, A.; Christianen, P. C.; Schüller, C.; Korn, T. Giant magnetic

splitting inducing near-unity valley polarization in van der Waals heterostructures. *Nature Communications* **2017**, *8*, 1–6.

(22) Förg, M.; Baimuratov, A. S.; Kruchinin, S. Y.; Vovk, I. A.; Scherzer, J.; Förste, J.; Funk, V.; Watanabe, K.; Taniguchi, T.; Högele, A. Moiré excitons in MoSe2-WSe2 heterobilayers and heterotrilayers. *Nature Communications* **2021**, *12*, 1–7.

(23) Baek, H.; Brotons-Gisbert, M.; Koong, Z.; Campbell, A.; Rambach, M.; Watanabe, K.; Taniguchi, T.; Gerardot, B. D. Highly energy-tunable quantum light from moiré-trapped excitons. *Science advances* **2020**, *6*, eaba8526.

(24) Huang, D.; Choi, J.; Shih, C.-K.; Li, X. Excitons in semiconductor moiré superlattices. *Nature Nanotechnology* **2022**, 1–12.

(25) Rivera, P.; Yu, H.; Seyler, K. L.; Wilson, N. P.; Yao, W.; Xu, X. Interlayer valley excitons in heterobilayers of transition metal dichalcogenides. *Nature Nanotechnology* **2018**, *13*, 1004–1015.

(26) Tartakovskii, A. Excitons in 2D heterostructures. *Nature Reviews Physics* **2020**, *2*, 8–9.

(27) Kuwabara, M.; Clarke, D. R.; Smith, D. Anomalous superperiodicity in scanning tunneling microscope images of graphite. *Applied physics letters* **1990**, *56*, 2396–2398.

(28) Seyler, K. L.; Rivera, P.; Yu, H.; Wilson, N. P.; Ray, E. L.; Mandrus, D. G.; Yan, J.; Yao, W.; Xu, X. Signatures of moiré-trapped valley excitons in MoSe 2/WSe 2 heterobilayers. *Nature* **2019**, *567*, 66–70.

(29) Förg, M.; Baimuratov, A. S.; Kruchinin, S. Y.; Vovk, I. A.; Scherzer, J.; Förste, J.; Funk, V.; Watanabe, K.; Taniguchi, T.; Högele, A. Moiré excitons in MoSe 2-WSe 2 heterobilayers and heterotrilayers. *Nature communications* **2021**, *12*, 1–7.

(30) Woźniak, T.; Junior, P. E. F.; Seifert, G.; Chaves, A.; Kunstmann, J. Exciton g factors of van der Waals heterostructures from first-principles calculations. *Physical Review B* **2020**, *101*, 235408.

(31) Deilmann, T.; Krüger, P.; Rohlfing, M. Ab initio studies of exciton g factors: monolayer transition metal dichalcogenides in magnetic fields. *Physical review letters* **2020**, *124*, 226402.

(32) Chen, S.-Y.; Lu, Z.; Goldstein, T.; Tong, J.; Chaves, A.; Kunstmann, J.; Cavalcante, L.; Wozniak, T.; Seifert, G.; Reichman, D., et al. Luminescent emission of excited Rydberg excitons from monolayer WSe2. *Nano letters* **2019**, *19*, 2464–2471.

(33) Tang, Y.; Gu, J.; Liu, S.; Watanabe, K.; Taniguchi, T.; Hone, J.; Mak, K. F.; Shan, J. Tuning layer-hybridized moiré excitons by the quantum-confined Stark effect. *Nature Nanotechnology* **2021**, *16*, 52–57.

(34) Alexeev, E. M.; Ruiz-Tijerina, D. A.; Danovich, M.; Hamer, M. J.; Terry, D. J.; Nayak, P. K.; Ahn, S.; Pak, S.; Lee, J.; Sohn, J. I., et al. Resonantly hybridized excitons in moiré superlattices in van der Waals heterostructures. *Nature* **2019**, *567*, 81–86.

(35) Zhang, L.; Zhang, Z.; Wu, F.; Wang, D.; Gogna, R.; Hou, S.; Watanabe, K.; Taniguchi, T.; Kulkarni, K.; Kuo, T., et al. Twist-angle dependence of moiré excitons in WS 2/MoSe 2 heterobilayers. *Nature communications* **2020**, *11*, 5888.

(36) Ma, X.; Fu, S.; Ding, J.; Liu, M.; Bian, A.; Hong, F.; Sun, J.; Zhang, X.; Yu, X.; He, D. Robust Interlayer Exciton in WS2/MoSe2 van der Waals Heterostructure under High Pressure. *Nano Letters* **2021**, *21*, 8035–8042, PMID: 34605657.

(37) *See Supplemental Material for additional measurements at different positions in the sample*

(38) Tran, K.; Moody, G.; Wu, F.; Lu, X.; Choi, J.; Kim, K.; Rai, A.; Sanchez, D. A.; Quan, J.; Singh, A., et al. Evidence for moiré excitons in van der Waals heterostructures. *Nature* **2019**, *567*, 71–75.

(39) Haastrup, S.; Strange, M.; Pandey, M.; Deilmann, T.; Schmidt, P. S.; Hinsche, N. F.; Gjerding, M. N.; Torelli, D.; Larsen, P. M.; Riis-Jensen, A. C., et al. The Computational 2D Materials Database: high-throughput modeling and discovery of atomically thin crystals. *2D Materials* **2018**, *5*, 042002.

(40) Tang, Y.; Gu, J.; Liu, S.; Watanabe, K.; Taniguchi, T.; Hone, J. C.; Mak, K. F.; Shan, J. Dielectric catastrophe at the Mott and Wigner transitions in a moir\'e superlattice. *arXiv preprint arXiv:2201.12510* **2022**,

(41) Koperski, M.; Molas, M. R.; Arora, A.; Nogajewski, K.; Bartos, M.; Wyzula, J.; Vaclavkova, D.; Kossacki, P.; Potemski, M. Orbital, spin and valley contributions to Zeeman splitting of excitonic resonances in MoSe2, WSe2 and WS2 Monolayers. *2D Materials* **2019**, *6*.

TOC Graphic

Some journals require a graphical entry for the Table of Contents. This should be laid out "print ready" so that the sizing of the text is correct.
Inside the `tocentry` environment, the font used is Helvetica 8 pt, as required by *Journal of the American Chemical Society*.
The surrounding frame is 9 cm by 3.5 cm, which is the maximum permitted for *Journal of the American Chemical Society* graphical table of content entries. The box will not resize if the content is too big: instead it will overflow the edge of the box.
This box and the associated title will always be printed on a separate page at the end of the document.